The Effect of Various Parameters of Circular Microstrip Antennas on Their Radiation Efficiency and the Mode Excitation

A. A. KISHK, STUDENT MEMBER, IEEE, AND LOTFOLLAH SHAFAI, SENIOR MEMBER, IEEE

Abstract—**The numerical solution of circular microstrip antenna is carried out using the method of moment. The effect of the probe position, The dielectric permittivity of the substrate, and the substrate thickness on the radiation pattern and the mode excitation efficiency are studied. It is found that the probe position and the patch size can be used to control the mode excitation efficiency, and heigher order modes can be generated using only one feed location. Also, the finite ground plane can be used to improve the symmetry of the radiation patterns. The technique is general and can be used to investigate other scattering and antenna problems involving axisymmetric geometries.**

INTRODUCTION

MICROSTRIP ANTENNAS are one of the most popular antenna types, since they are lightweight, have simple geometries, are inexpensive to fabricate and can be easily made conformal to the host body. These attractive features have increased their application recently and stimulated an ever increasing effort to investigate their performance. The analysis of the microstrip antenna is normally difficult to handle, which is primarily due to the existence of a dielectric substrate to support the conductor. Early studies have therefore been focused on developing approximate methods, such as the transmission line model [1], [2], cavity model [3], [4], modal analysis [5], [6] and a full wave analysis method for the rectangular [7] and for circular geometries [8]. A numerical method was developed by Newman [9] using the moment method with the image theory to calculate the input impedance of a rectangular patch. Shortly after Baily and Deshpande [10], [11] used the same technique to calculate the input impedance using an exact dyadic Green's function. Each method has made a certain approximation to simplify the problem and in particular has obtained solutions for an infinite substrate and ground plane geometry, which is not the case practically.

In this paper, a rigorous treatment of the problem is carried out using a numerical method applicable to circular microstrip patch geometries. Integral equations are developed which are valid for a multiple region problem consisting of dielectrics and conductors. These integral equations are then applied to rotationally symmetric objects and reduced to a matrix equation using the procedure common in solving the problem of bodies of revolution [12], [13]. When the method is applied to a circular microstrip antenna, it provides a convenient approach to solve for the contribution of various modes that are present in the structure and correspond to those of the modal expansion method. The difference, however, is that here the excitation efficiency of each mode can be determined accurately, and each mode's radiation patterns in combined or individual forms can be calculated. Also, the effect of the geometrical and physical parameters of the the antenna such as the patch size, substrate permittivity and height, and the size of the ground plane on the mode resonances and their relative magnitude can be determined. The number and location of the excitation probes are also significant to the relative intensity of the modes and their effects can be studied by the present method.

Manuscript received September 7, 1985; revised February 25, 1986.

The authors are with the Department of Electrical Engineering, University of Manitoba, Winnipeg, Manitoba, R3T 2N2, Canada.

IEEE Log Number 8609027.

FORMULATION OF THE PROBLEM

The formulation of the problem is in terms of the surface integral equations. These equations are exact. Consequently, the accuracy of the solution depends on the nature of the numerical technique selected to solve them. The derivation of the equations governing the problem may be based on the equivalence principle [11], [12]. Fig. 1(a) shows the general electromagnetic problem under consideration, where a dielectric object is partially coated with a conductor. The surfaces S_{ce}, S_{cd}, and S_{de} refer, respectively to the boundaries between the conductor and the exterior region, conductor and dielectric, and dielectric and the exterior region. Also, $\vec{E}^d$, $\vec{H}^d$ and $\vec{E}^e$, $\vec{H}^e$ refer to the field vectors within the dielectric and the exterior regions, respectively.

In Fig. 1(a), V^d is a finite volume filled with a homogeneous material of permittivity ϵ_d and permeability μ_d and bounded by two surfaces S_{de} and S_{cd}. The surface S_{cd} may consist of several subsurfaces, to represent multiple dielectric and conducting interfaces. V^e represents the external region, with a permittivity of ϵ_e and permeability of μ_e, and is bounded by two surfaces S_{de} and S_{ce}. Again, the surface S_{ce} may consist of several subsurfaces. In the present work, all these surfaces are assumed to be rotationally symmetric, to represent bodies of revolution. The sources of the electromagnetic excitation are provided by the impressed electric and magnetic currents $\vec{J}^{id}$ and $\vec{M}^{id}$ in V^d.

The equivalence principle [14] is used to obtain the auxiliary problems shown in Figs. 1(b) and 1(c). In Fig. 1(b), the equivalent currents $\vec{J}_{ce}$, $\vec{J}_{de}$, and $\vec{M}$ radiate in the presence of the homogeneous medium (μ_e, ϵ_e) to produce ($\vec{E}^e$, $\vec{H}^e$) in V^e

0018-926X/86/0800-0969$01.00

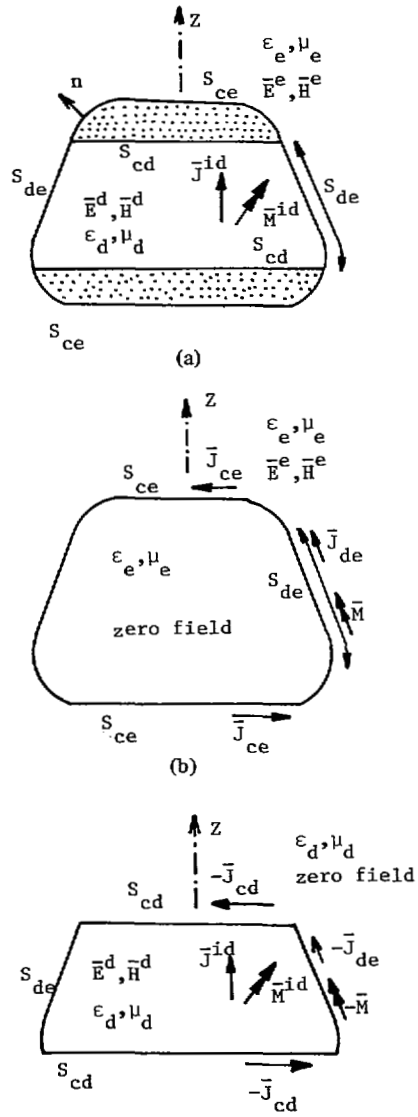

Fig. 1. Problem representation by equivalence principle. (a) Original problem. (b) External equivalence. (c) Internal equivalence.

and zero field elsewhere. Here, $\vec{J}_{ce}$ is an electric current on S_{ce}, $\vec{J}_{de}$ is an electric current on S_{de}, and $\vec{M}$ is a magnetic current on S_{de}. In Fig. 1(c), $(\vec{J}^{id}, \vec{M}^{id})$ and equivalent currents $-\vec{J}_{cd}$, $-\vec{J}_{de}$, and $-\vec{M}$ radiate in the presence of the homogeneous medium (μ_d, ϵ_d) to produce $(\vec{E}^d, \vec{H}^d)$ in V^d and zero field elsewhere. Here, $-\vec{J}_{cd}$ is the electric current on S_{cd}, $-\vec{J}_{de}$ is an electric current on S_{de}, and $-\vec{M}$ is a magnetic current on S_{de}. Since the surfaces S_{ce} and S_{cd} are perfectly conducting in the original problem of Fig. 1(a), only equivalent electric currents are needed on them in Figs. 1(b) and 1(c). The choice of $-\vec{J}_{cd}$ rather than $\vec{J}_{cd}$ on S_{cd} in Fig. 1(c) depends on a personal preference. However, the minus sign relationship between the aperture currents in Figs. 1(b) and 1(c) is dictated by the zero field stipulations in Figs. 1(b) and 1(c) and the continuity of the tangential components of the electric and magnetic fields across the aperture in Fig. 1(a). If the zero field stipulations in Figs. 1(b) and 1(c) are enforced, then the minus sign relationship between the aperture currents in these figures ensures the continuity of the tangential fields across the aperture.

The equivalence principle states that the equivalent currents in Figs. 1(b) and 1(c) are unique, but it does not indicate their evaluation method. The expressions in [14] for the equivalent currents in terms of the tangential components of the fields can not be used, since the fields are not known. The equivalent currents can be determined by enforcing the boundary conditions for the fields in Fig. 1(a) as in [15]. These surface equivalent currents are

$$\vec{J}_{cd} = \hat{n} \times \vec{H}^d, \qquad \text{on } S_{cd} \tag{1}$$

$$\vec{J}_{ce} = \hat{n} \times \vec{H}^e, \qquad \text{on } S_{ce} \tag{2}$$

$$\vec{J}_{de} = \hat{n} \times \vec{H}^e, \quad \vec{M} = -\hat{n} \times \vec{E}^e, \qquad \text{on } S_{de}. \tag{3}$$

Again, the currents $\vec{J}_{cd}$, $\vec{J}_{ce}$, and $\vec{J}_{de}$ are the equivalent electric currents on each respective surface, and $\vec{M}$ is the magnetic current on the interface surface between the dielectric and the exterior region. The boundary conditions can be written as

$$-\frac{1}{\eta_e} \vec{E}^d_{\tan}(\vec{J}_{cd} + \vec{J}_{de},\ \vec{M}) = -\frac{1}{\eta_e} \vec{E}^d_{\tan}(\vec{J}^{id},\ \vec{M}^{id}), \qquad \text{on } S_{cd} \tag{4}$$

$$-\frac{1}{\eta_e} \vec{E}^e_{\tan}(\vec{J}_{ce} + \vec{J}_{de},\ \vec{M}) = 0, \qquad \text{on } S_{ce} \tag{5}$$

$$-\frac{1}{\eta_e} \vec{E}^e_{\tan}(\vec{J}_{ce} + \vec{J}_{de},\ \vec{M}) - \frac{1}{\eta_e} \vec{E}^d_{\tan}(\vec{J}_{cd} + \vec{J}_{de},\ \vec{M}) = -\frac{1}{\eta_e} \vec{E}^d_{\tan}(\vec{J}^{id},\ \vec{M}^{id}), \qquad \text{on } S_{de} \tag{6}$$

$$-\vec{H}^e_{\tan}(\vec{J}_{ce} + \vec{J}_{de},\ \vec{M}) - \vec{H}^d_{\tan}(\vec{J}_{cd} + \vec{J}_{de},\ \vec{M}) = -\vec{H}^d_{\tan}(\vec{J}^{id},\ \vec{M}^{id}), \qquad \text{on } S_{de} \tag{7}$$

where $\vec{E}^e_{\tan}(\vec{J}, \vec{M})$ and $\vec{E}^d_{\tan}(\vec{J}, \vec{M})$ are the tangential components of the electric fields due to currents $\vec{J}$ and $\vec{M}$, radiating in media characterized by ϵ_e, μ_e and ϵ_d, μ_d, respectively. $\vec{H}^e_{\tan}(\vec{J}, \vec{M})$ and $\vec{H}^d_{\tan}(\vec{J}, \vec{M})$ denote the tangential components of the corresponding magnetic fields. These equations are dependent on the scalar Green's function G^q, which is given by

$$G^q = \frac{\exp(-jk_q R)}{4\pi R} \tag{8}$$

where $R = |\vec{r} - \vec{r}'|$ is the distance between the field point $\vec{r}$ and the source point $\vec{r}'$ on the surface, $k_q = \omega(\epsilon_q \mu_q)^{1/2}$ is the propagation constant and q represents e or d.

Matrix Formulations

The reduction of integral equations to matrix equations involving unknown surface currents follows the procedure well known for bodies of revolution. Here, both electric and magnetic surface currents exist and are represented by Mautz and Harrington [12], [13] and Iskander *et al.* [16] as

$$\vec{J}(\vec{r}') = \hat{u}_t J^t(t,\ \phi) + \hat{u}_\phi J^\phi(t,\ \phi) \tag{9}$$

$$\vec{M}(\vec{r}') = \hat{u}_t M^t(t,\ \phi) + \hat{u}_\phi M^\phi(t,\ \phi) \tag{10}$$

where $\hat{u}_t$ and $\hat{u}_\phi$ are the unit tangents to the body as in [9] and J^t, J^ϕ and M^t, M^ϕ are the current components. The electric current $\vec{J}$ exists on both conducting and dielectric surfaces, but $\vec{M}$ exists only on the dielectrics. If the electric and the magnetic currents are expanded into Nc and Nd expansion functions, respectively, the surface currents can be represented as

$$\vec{J}(\vec{r}) = \sum_{n=-M0}^{M0} \sum_{j=1}^{Nc} I^t_{nj} J^t_{nj}(t, \phi)\hat{u}_t + I^\phi_{nj} J^\phi_{nj}(t, \phi)\hat{u}_\phi \quad (11)$$

$$\vec{M}(\vec{r}) = \eta_e \sum_{n=-M0}^{M0} \sum_{j=Nc+1}^{Nc+Nd} M^t_{nj} K^t_{nj}(t, \phi)\hat{u}_t + M^\phi_{nj} K^\phi_{nj}(t, \phi)\hat{u}_\phi \quad (12)$$

where J^t_{nj}, J^ϕ_{nj}, K^t_{nj}, K^ϕ_{nj} are expansion functions defined as

$$J^t_{nj} = J^\phi_{nj} = K^t_{nj} = K^\phi_{nj} = f_j(t)e^{jn\phi} \quad (13)$$

The range $-M0$ to $+M0$ gives the total number of azimuthal modes. The coefficients I^t_{nj}, I^ϕ_{nj}, M^t_{nj}, M^ϕ_{nj} are the current coefficients to be determined by solving the matrix equation which results when (11) and (12) are substituted into (4) to (7) and the inner product, integrated over the surface, of the resulting equation with testing functions $\vec{W}^t_{li}$ and $\vec{W}^\phi_{li}$ are carried out. The testing functions are

$$\vec{W}^t_{li} = \hat{u}_t f_i(t)e^{-jl\phi} \quad (14)$$

$$\vec{W}^\phi_{li} = \hat{u}_\phi f_i(t)e^{-jl\phi} \quad (15)$$

and the details of above steps are provided in [12], [13].

The general matrix form takes the form

$$[\bar{T}_n][\bar{I}_n] = [\bar{V}_n], \quad n = 0, \pm 1, \pm 2, \cdots \quad (16)$$

where $\bar{T}_n$ is a square matrix, representing the impedance and the admittance submatrices, $\bar{I}_n$ is a column matrix for the unknown expansion coefficients of $\vec{J}$ and $\vec{M}$, and $\bar{V}_n$ is the excitation column matrix. Each mode has a matrix equations of the form

$$\begin{bmatrix} Z^e_{ce,ce} & 0 & Z^e_{ce,de} & Y^e_{ce,de} \\ 0 & \eta_r Z^d_{cd,cd} & \eta_r Z^d_{cd,de} & Y^d_{cd,de} \\ Z^e_{de,ce} & \eta_r Z^d_{de,cd} & Z^e_{de,de} + \eta_r Z^d_{de,de} & Y^e_{de,de} + Y^d_{de,de} \\ Y^e_{de,ce} & Y^d_{de,cd} & Y^e_{de,de} + Y^d_{de,de} - Z^e_{de,de} - \dfrac{1}{\eta_r} & Z^d_{de,de} \end{bmatrix} \begin{bmatrix} I_{ce,n} \\ I_{cd,n} \\ I_{de,n} \\ M_{de,n} \end{bmatrix} = \begin{bmatrix} 0 \\ -V^d_{cd,n} \\ -V^d_{de,n} \\ -I^d_{de,n} \end{bmatrix} \quad (17)$$

where $\eta_r = \eta_d/\eta_e$ and $V^d_{cd,n}$, $V^d_{de,n}$ and $I^d_{de,n}$ are the excitation submatrices, due to the electric and magnetic field sources on the surfaces S_{cd}, S_{de} from the interior region, respectively. The submatrices Z and Y with superscripts e and d denote the impedance and admittance matrices for the exterior or interior media, respectively, the first and second pairs of suffixes identify the field and source surfaces, and the index n implies azimuthal mode number. $I_{ce,n}$, $I_{cd,n}$, $I_{de,n}$ and $M_{de,n}$ are the unknown expansion coefficients of the electric and magnetic currents on S_{ce}, S_{cd}, and S_{de} respectively. In the above equations, each submatrix Y^q or Z^q consists of four submatrices, which are obtained by the procedure used in [9].

Excitation Matrix

For the microstrip problem the coaxial feed probe is simulated by an electric dipole in the dielectric substrate. The electric and magnetic fields due to an electric dipole are

$$\vec{E}^{\text{inc},q} = -j\omega\vec{A}^q - \nabla\Phi^q \quad (18)$$

$$\vec{H}^{\text{inc},q} = -\frac{1}{\mu_q}\nabla\times\vec{A}^q \quad (19)$$

where

$$\vec{A}^q = \frac{-jk_q\mu_q}{4\pi r}\vec{I}l\ h^{(2)}_0(k_q|\vec{r}-\vec{r}'|) \quad (20)$$

$$\Phi^q = \frac{\eta_q}{4\pi r}\vec{I}l\cdot\nabla h^{(2)}_0(k_q|\vec{r}-\vec{r}'|) \quad (21)$$

and $h^{(2)}_0$ is the spherical Hankel function of the second kind and zero order and $\vec{I}l$ is the dipole moment, in the z-direction. If the Hankel function is represented by

$$h^{(2)}_0(k_q|\vec{r}-\vec{r}'|) = \sum_{-\infty}^{\infty} G_m e^{jm(\phi-\phi)} \quad (22)$$

with

$$G_m = G_{-m} = \begin{cases} \displaystyle\sum_{n=m}^{\infty} a_n h^{(2)}_n(k_q r')j_n(K_q r)P^m_n(\cos\theta)P^m_n(\cos\theta'), & r' > r \\ \displaystyle\sum_{n=m}^{\infty} a_n h^{(2)}_n(k_q r)j_n(k_q r')P^m_n(\cos\theta)P^m_n(\cos\theta'), & r' < r \end{cases} \quad (23)$$

where $a_n = (2n+1)(n-m)!/(n+m)!$, the inner products of $\vec{E}^{\text{inc}}$ and $\vec{H}^{\text{inc}}$ with testing functions $\vec{W}_{li}$ provide the elements of the excitation matrix. This column matrix has the elements in the form

$$(V^q_m)^t_{iz} = (\eta_q|Il|_z/2)\left[-k_q^2\int_0^{tu} dt\ \rho f_i(t) \cdot\cos\nu G_m - \int_0^{tu} dt\,\frac{d}{dt}(\rho f_i(t))\frac{1}{\rho}\frac{\partial G_m}{\partial\theta}\right] \quad (24)$$

$$(V^q_m)^\phi_{iz} = (\eta_q|Il|_z/2)\left(jm\int_0^{tu} dt\,\frac{1}{\rho}f_i(t)\frac{\partial G_m}{\partial\theta}\right) \quad (25)$$

$$(I_m^q)_{iz_t} = (-jk_q|Il|_z/2) \int_0^{tu} dt\, f_i(t) \sin \nu G_m \quad (26)$$

$$(I_m^q)_{iz}^{\phi} = (-jk_q|Il|_z/2) - \int_0^{tu} dt\, \rho f_i(t) \frac{\partial G_m}{\partial r} \quad (27)$$

where ρ is the distance from the field point on the surface to the Z-axis and v is the angle between the Z-axis and the unit tangent t at the field point.

The Measurement Coefficients

Once the induced currents $\vec{J}$ and $\vec{M}$ on the surface are determined after the solution of the matrix equations, the far-field components E_θ and E_ϕ at a far-field point (r_0, θ_0, ϕ_0) can be determined [17] as

$$E_\theta = \frac{-j\omega\mu_e}{4\pi r_0} e^{-jkr_0} F_1(\theta_0, \phi_0) \quad (28)$$

$$E_\phi = \frac{-j\omega\mu_e}{4\pi r_0} e^{-jkr_0} F_2(\theta_0, \phi_0) \quad (29)$$

where F_1 and F_2 are the measurement coefficients in this form

$$F_1(\theta_0, \phi_0) = \int_s \left(\vec{J} \cdot \hat{u}_\theta + \frac{1}{\eta_e} \vec{M} \cdot \hat{u}_\phi \right) e^{-jk_e \hat{r}_0 \cdot \vec{r}'} ds \quad (30)$$

$$F_2(\theta_0, \phi_0) = \int_s \left(\vec{J} \cdot \hat{u}_\phi - \frac{1}{\eta_e} \vec{M} \cdot \hat{u}_\theta \right) e^{-jk_e \hat{r}_0 \cdot \vec{r}'} ds \quad (31)$$

where S is the total outer surface of the body, $\hat{r}_0$ is a unit vector in the direction from the origin of the coordinates to the field point, $\vec{r}'$ is the positional vector of the source point (x', y', z') on the body, and $\hat{u}_\theta$ and $\hat{u}_\phi$ are unit vectors in the direction of increasing θ and ϕ, respectively. Note that E_θ and E_ϕ are the total fields in the exterior region.

Results and Discussions

The antenna geometry for a circular microstrip antenna with a finite ground plane is shown in Fig. 2, where the excitation is simulated by an electric dipole immersed in the dielectric substrate under the conducting patch. The patch radius, for all data in this paper, is selected as [4]

$$a_e = \left[1 + \frac{2h}{\pi a \epsilon_r} \left(\ln \frac{\pi a}{2h} + 1.7726 \right) \right]^{1/2} \quad (32)$$

where a is the actual radius of the conducting patch, a_e is the effective radius due to the spread of the fringing field from the patch edge to the ground plane, h is the dielectric thickness and ϵ_r is the relative permittivity of the dielectric substrate. The effective radius is calculated from

$$a_e = \frac{K_{nm}}{2\pi\sqrt{\epsilon_r}} \quad (33)$$

where K_{nm} is the mth zero of the derivative of the Bessel function of order n.

In this paper the patch size is selected according to (32) together with (33) which are functions of the substrate height,

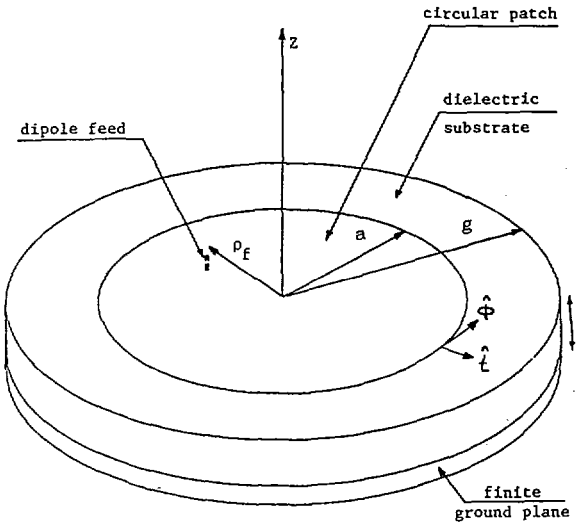

Fig. 2. Microstrip antenna geometry.

the dielectric permittivity, and the desired mode of excitation. For each selected patch size the effects of other parameters on the antenna performance are studied and summarized in the following sections.

A. Feed Location

For coaxial feeds, location is usually selected to provide a good impedance match. Here, the dipole location is selected to ensure the proper excitation of the required mode. Fig. 3 shows the effect of the feed position ρ_f on the excitation efficiency for the TM_{11} mode. In this figure the peaks of the radiation patterns of TM_{01}, TM_{11}, TM_{21} modes are plotted to indicate their relative excitation level. The dominant mode is the strongest for all feed locations and the influence of the TM_{01} and TM_{21} modes increases by moving the feed toward the patch edge. It is evident that increasing the substrate thickness increases the influence of the TM_{01} and TM_{21} modes and decreases the relative excitation of the dominant mode. The excitation of the TM_{21} mode is shown in Fig. 4. Moving the feed away from the patch center increases the excitation of the TM_{21} mode initially, but decreases its excitation for $\rho_f > 0.68\ a$. The excitation of the other modes oscillate around a certain range, which depends on the order of each mode. Although the TM_{21} mode has the highest excitation at $\rho_f = 0.68\ a$, its relative excitation, with respect to the other modes, is strongest around $\rho_f = 0.75\ a$. The effect of the substrate permittivity was found to be insignificant. These results indicate that the excitation of TM_{11} or TM_{21} modes can be controlled by the feed location alone and in principle multiple feed locations are not necessary to excite higher order modes.

The radiation patterns of circular patchs for the dominant TM_{11} and TM_{21} modes excitation are shown in Fig. 5. The patterns for TM_{11} mode are calculated by including the contributions of the first four TM_{01}, TM_{11}, TM_{21}, and TM_{31} modes and the patterns for the TM_{21} mode are calculated by including the first five modes, TM_{01}, TM_{11}, TM_{21}, TM_{31} and TM_{41} modes. In each case the feed locations are selected to optimize the dominant mode excitation and the TM_{21} mode excitation, respectively. One example is selected to compare

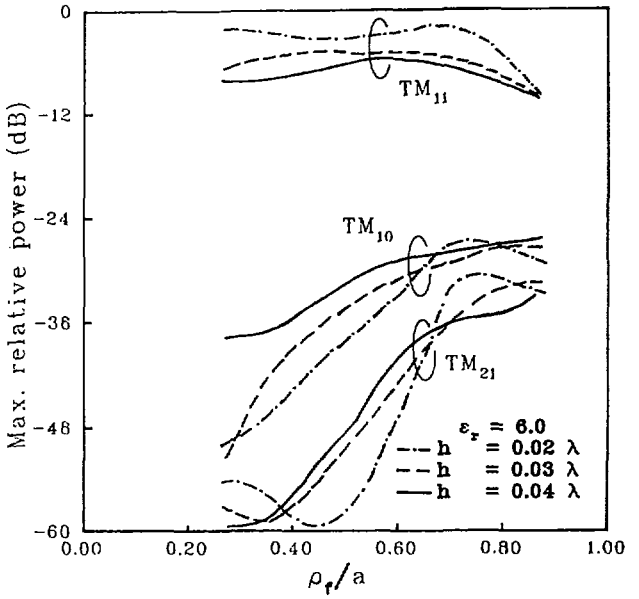

Fig. 3. The effect of the feed position on the excitation efficiency of TM_{11} mode.

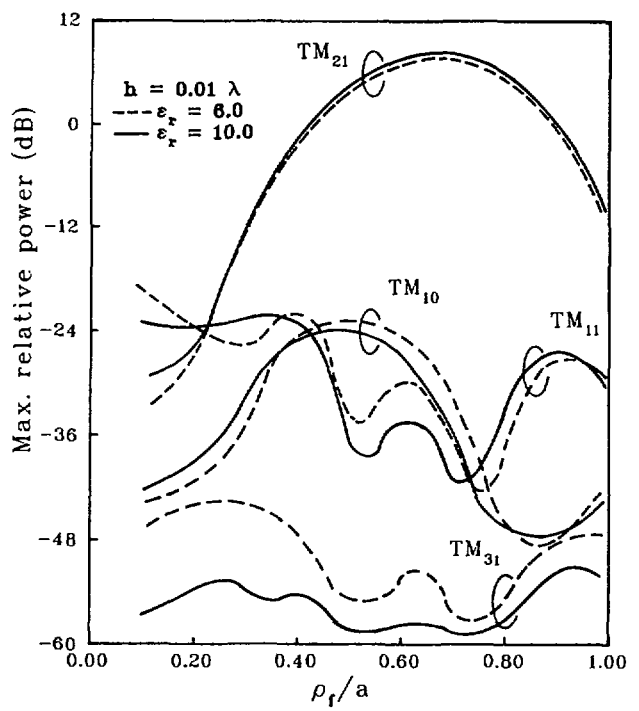

Fig. 4. The effect of the feed position on the excitation efficiency of TM_{21} mode.

the computed and the measured data as shown in Fig. 6 with the ground plane $g = 0.5\ \lambda$. Excellent agreement between the measured and computed data was found.

In practice, it is also desirable to understand the nature of radiation from a microstrip patch antenna. In the past, it was assumed that the fringing field near the patch edge is responsible for the radiations. To investigate this, the surface currents are also determined and plotted for both TM_{11} and TM_{21} modes. Fig. 7 shows the computed electric and magnetic surface currents for the TM_{11} mode on the outer boundary of

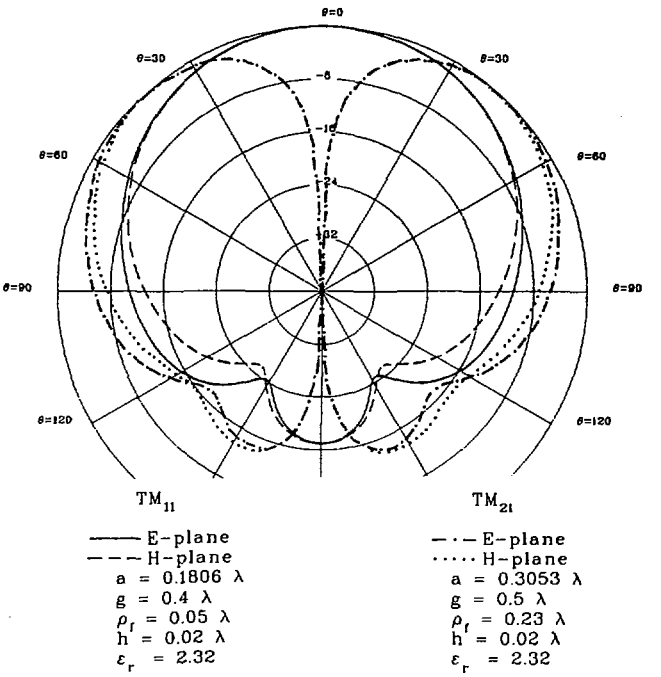

Fig. 5. The radiation patterns of a circular patch for the TM_{11} and TM_{21} mode excitations.

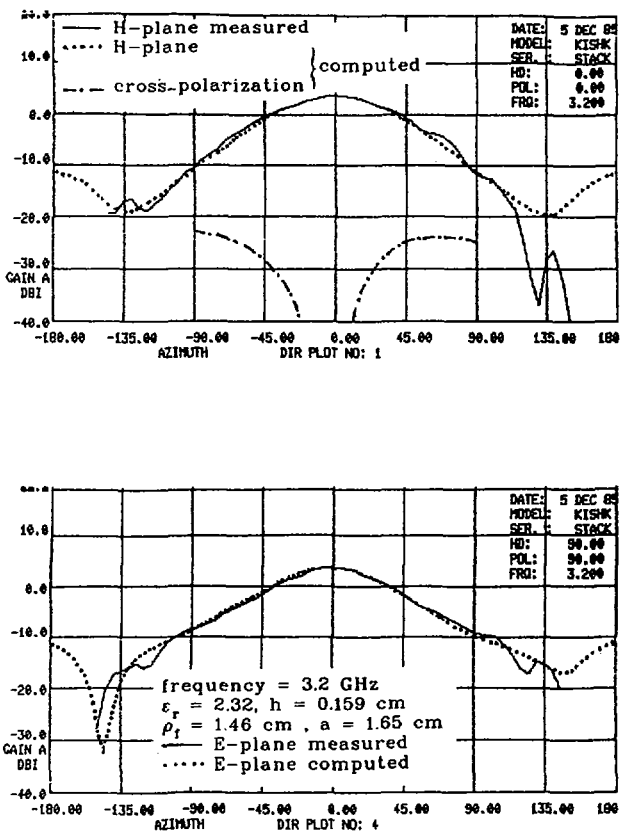

Fig. 6. Experimental and computed data of a circular patch excited with a coaxial probe.

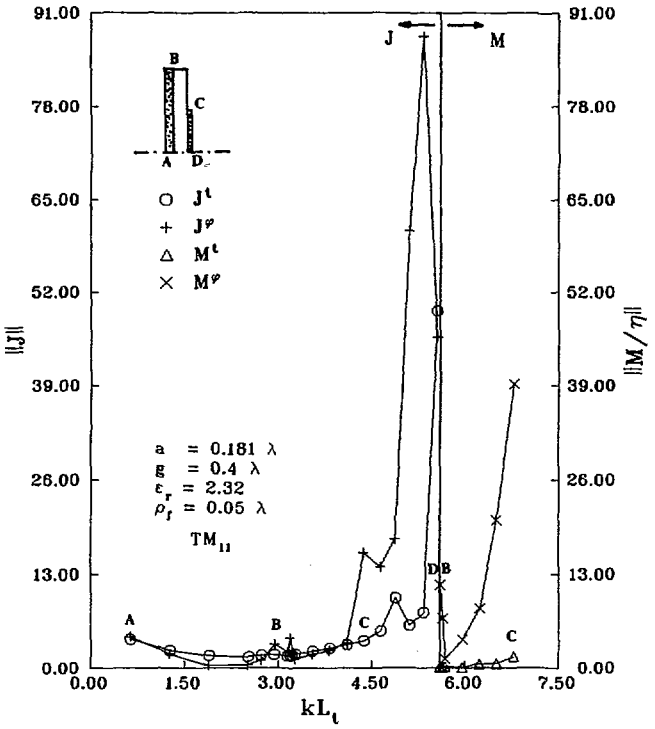

Fig. 7. The computed electric and magnetic surface currents of the TM_{11} mode on the outside boundary.

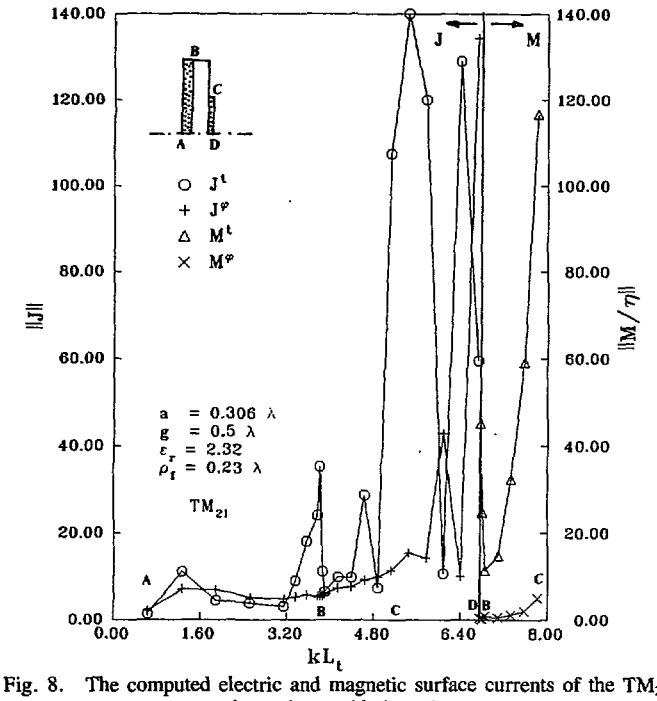

Fig. 8. The computed electric and magnetic surface currents of the TM_{21} mode on the outside boundary.

the microstrip surface. Due to the structure symmetry, only half of the geometry is considered as shown in Fig. 7. In this figure the currents are plotted with respect to its locations of the surface and the points A to B correspond to the ground plane, the points B to C correspond to the dielectric substrate which has electric and magnetic currents and C to D correspond to the patch surface. L_t represent the contour length. The magnetic current M^ϕ is considerably stronger than M^t and is maximum near the patch edge. It reduces towards the dielectric edge, but rises again on its end surface. This indicates that the main radiation comes from the dielectric surface near the patch edge, its truncated end face, and the electric current on the upper patch surface. The corresponding results for the TM_{21} mode are shown in Fig. 8. The main radiation zones are the same as the dominant mode case.

B. The Effect of the Substrate Permittivity

The effect of the substrate permittivity is shown in Fig. 9, which presents the radiation patterns of a circular patch with the dominant mode in resonance. The upper part shows the H-plane and cross-polar patterns and the lower one the E-plane patterns. It can be seen that the beamwidth increases with ϵ_r, but the effect of ϵ_r is stronger on the E-plane than on the H-plane. As a result, increasing the permittivity of the substrates deteriorates the symmetry of the radiation patterns and consequently increases the cross-polar level.

C. Effect of the Substrate Thickness

The bandwidth of microstrip antennas normally increases by increasing the substrate thickness. It is therefore desirable

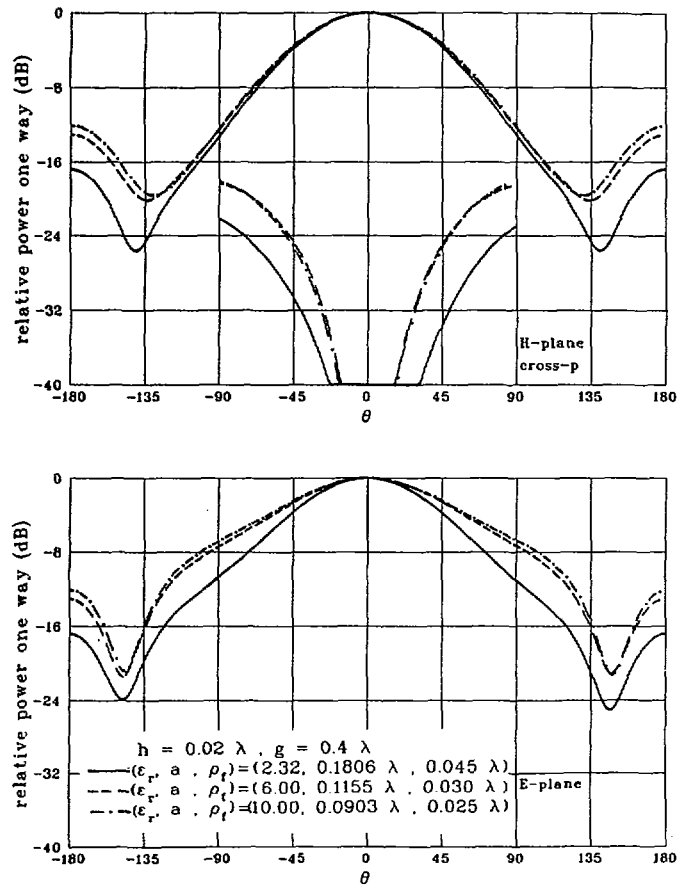

Fig. 9. The radiation pattern of a circular patch with different substrate permittivity.

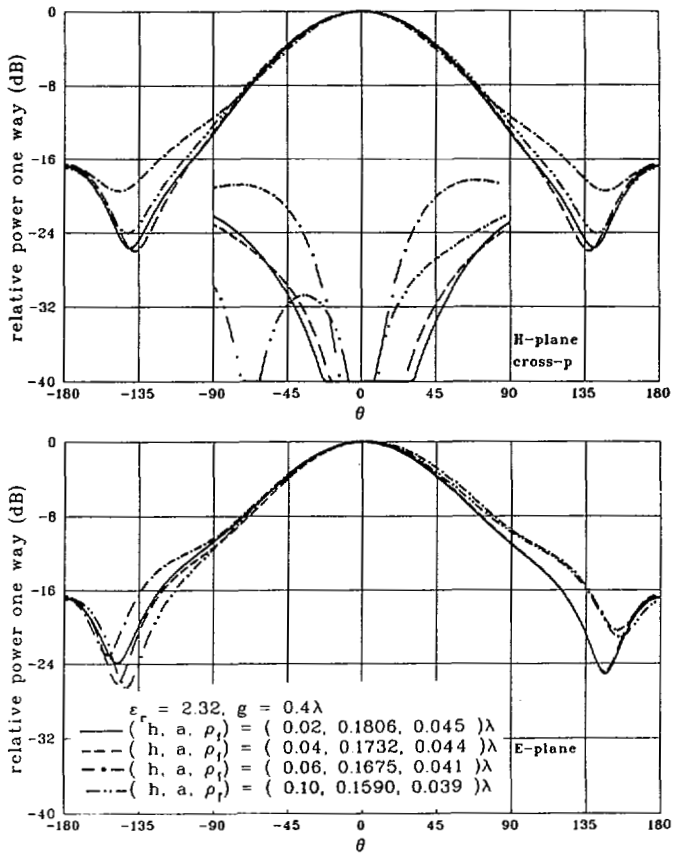

Fig. 10. The radiation patterns of a circular patch with different substrate height.

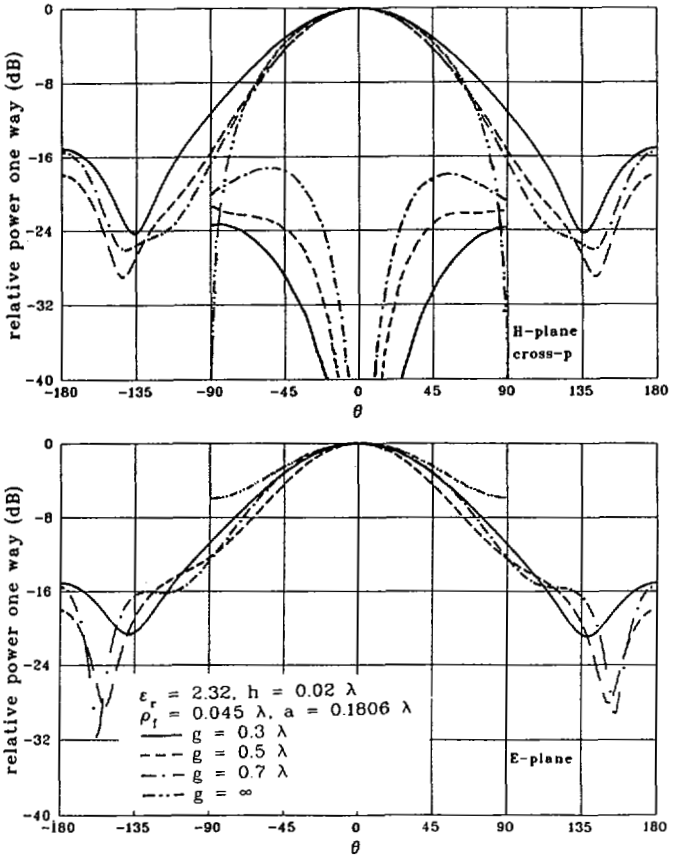

Fig. 11. The radiation patterns of a circular patch with different ground plane diameter for the dominant TM_{11} mode.

to study its effect on the radiation patterns. Fig. 10 shows the radiation patterns for a circular patch when TM_{11} is at resonance. It shows that increasing h increases the beamwidth in the E-plane, but reduces it in the H-plane, until h reaches 0.06 λ, after which the relationship reverses. The substrate thickness, generally, has a small effect on the radiation patterns.

D. Effect of the Ground Plane Size

The size of the ground plane has a pronounced effect on the far-field patterns. Fig. 11 shows its effect on the radiation patterns of a dominant TM_{11} mode patch, where the patterns for an infinite ground plane are calculated up to $\theta = 90°$. The results for an infinite ground plane are calculated using the image theory and truncating the dielectric at a radius of 0.4 λ. It seems that increasing the ground plane size increases the beamwidth of the E-plane patterns and decreases it for the H-plane patterns. This means the pattern symmetry can be improved by modifying the ground plane radius. The corresponding results for the TM_{21} mode are shown in Fig. 12, which are similar to the dominant mode case of Fig. 11. The radiation pattern are broader in the E-plane and tend to become narrow in the H-plane. Also, the difference between the peaks of the patterns in the E- and H-planes increases, and, the peaks move in opposite directions. For an infinite ground plane, the peaks move to $\theta = 52°$ and 42° for the E- and H-planes, respectively.

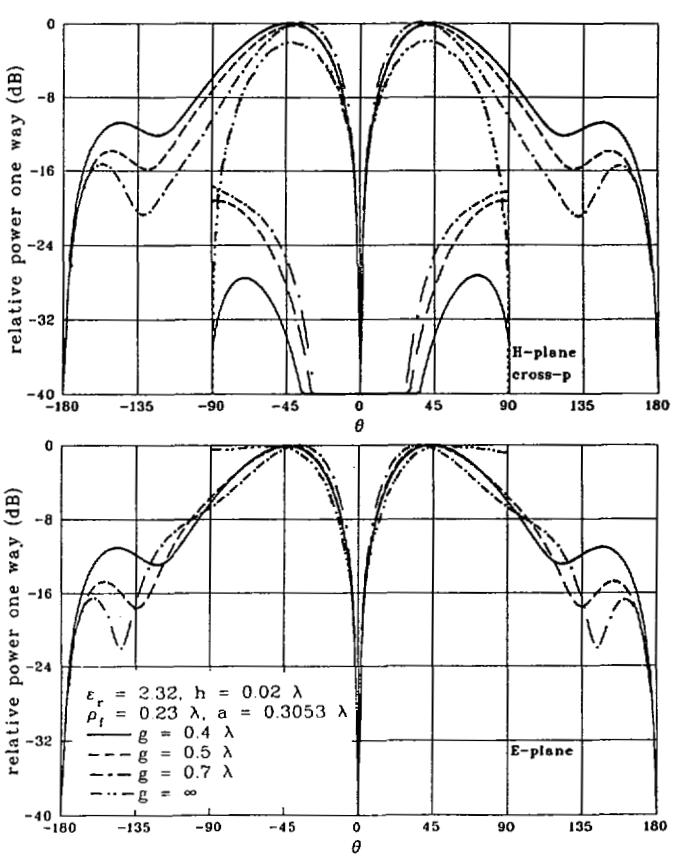

Fig. 12. The radiation patterns of a circular patch with different ground plane diameter for the TM_{21} mode.

Conclusion

The radiation characteristics of a circular microstrip patch antenna were studied numerically using the method of moment. The study included the effects of the finite ground plane, the substrate thickness, the feed locations and the material permittivity. The antenna geometry was considered as a multiple region problem, and the solution was obtained by applying the exact boundary conditions.

It was found that the feed location affects the excitation of each mode, and by its proper selection the resonant mode could be made dominant. In this manner the excitation of the higher order modes could be achieved using only a single feed location rather than multiple feed excitations. It was also shown that the ground plane size can be used to improve the pattern symmetry which is desirable for low cross polarization and circularly polarized applications. The permittivity of the substrate, also, could be used to reduce the physical dimension of the patch and to control the symmetry of the radiation patterns.

The method allowed us to study the effect of each mode separately and to determine their excitation efficiency. The technique can also be used to study the annular ring microstrip patch or annular slot antennas on a finite ground plane, as well as covered microstrip antennas and stacked multiple band configurations.

References

[1] R. E. Munson, "Conformal microstrip antennas and microstrip phased arrays," *IEEE Trans. Antennas Propagat.*, vol. AP-22, pp. 74–78, 1974.

[2] A. G. Derneryd, "Linearly polarized microstrip antennas," *IEEE Trans. Antennas Propagat.*, vol. AP-24, pp. 267–270, 1976.

[3] A. G. Derneryd and A. G. Lind, "Extended analysis of rectangular microstrip antennas," *IEEE Trans. Antennas Propagat.*, vol. AP-27, pp. 846–849, 1979.

[4] I. J. Bahl and R. Bhartia, *Microstrip Antennas*. Dedham, MA: Artech House, 1980.

[5] W. F. Richards, Y. T. Lo, and D. D. Harrison, "An improved theory for microstrip antennas and applications," *IEEE Trans. Antennas Propagat.*, vol. AP-29, pp. 38–46, 1981.

[6] S. Yano and A. Ishimaru, "A theoretical study of the input impedance of a circular disk antenna," *IEEE Trans. Antennas Propagat.*, vol. AP-29, pp. 77–83, 1981.

[7] T. Itoh and W. Menzel, "A full-wave analysis method for open microstrip structures," *IEEE Trans. Antennas Propagat.*, vol. AP-29, pp. 63–68, 1981.

[8] K. Araki and T. Itoh, "Hankel transform domain analysis of open circular microstrip radiating structures," *IEEE Trans. Antennas Propagat.*, vol. AP-29, pp. 84–89, 1981.

[9] E. D. Newman and P. Tulyathan, "Analysis of microstrip antennas using moment methods," *IEEE Trans. Antennas Propagat.*, vol. AP-29, pp. 47–53, 1981.

[10] M. C. Bailey and M. D. Deshpande, "Integral equation formulation of the microstrip antennas," *IEEE Trans. Antennas Propagat.*, vol. AP-30, pp. 651–656, 1982.

[11] M. D. Deshpande and M. C. Bailey, "Input impedance of microstrip antennas," *IEEE Trans. Antennas Propagat.*, vol. AP-30, pp. 645–650, 1982.

[12] J. R. Mautz and R. F. Harrington, "H-field, E-field, and combined field solutions for conducting bodies of revolution," *AEU* 32, 157–164.

[13] ——, "Electromagnetic scattering from a homogeneous material body of revolution," *AEU*, vol. 33, 71–80, 1979.

[14] R. F. Harrington, *Time-Harmonics Electromagnetic Fields*. New York: McGraw-Hill, 1961.

[15] J. R. Mautz and R. F. Harrington, "Boundary formulation for aperture coupling problem," *AEU*, vol. 34, 377–384, 1980.

[16] K. A. Iskander, L. Shafai, A. Frandsen and J. E. Hansen, "Application of impedance boundary conditions to numerical solution of corrugated circular horns," *IEEE Trans. Antennas Propagat.*, vol. AP-30, pp. 366–372, 1982.

[17] S. Silver, *Microwave Antenna Theory and Design*. New York: McGraw-Hill, 1949, pp. 87–89.

A. A. Kishk (S'83), for a photograph and biography please see page 673 of the May 1986 issue of this TRANSACTIONS.

Lotfollah Shafai (S'67–M'69–SM'75), for a photograph and biography please see page 673 of the May 1986 issue of this TRANSACTIONS.